SCIENCE CHINA
Chemistry

•ARTICLES•

https://doi.org/10.1007/s11426-024-2523-2

Aggregation of thermally activated delayed fluorescence molecules to boost solid electrochemiluminescence efficiency for biosensing of protein-specific glycoforms

Chao Wang[1], Zhiwei Tang[1], Yiran Li[1], Mengjiao Li[1], Haijiao Xie[2] & Huangxian Ju[1*]

[1]*State Key Laboratory of Analytical Chemistry for Life Science, School of Chemistry and Chemical Engineering, Nanjing University, Nanjing 210023, China*
[2]*Hangzhou Yanqu Information Technology Co., Ltd., Hangzhou 310003, China*

Received October 31, 2024; accepted January 9, 2025; published online February 6, 2025

Low quantum yield and insufficient exciton utilization of nanoemitters are great obstacles to achieving their practical electrochemiluminescence (ECL) applications. Here an aggregation strategy of thermally activated delayed fluorescence molecules was designed to reduce the energy gap between the lowest excited singlet and triplet states, and accelerate the reverse intersystem crossing of triplet excitons to the excited singlet state, which increased the exciton utilization, leading to longer delayed fluorescence lifetime and greatly boosted the quantum yield up to 87.5%, using a previously reported DMAC-TRZ as a model. The aggregation could be conveniently performed by increasing the water content in the tetrahydrofuran solution of DMAC-TRZ. Benefiting from the high quantum yield, the solid ECL efficiency was broken through to 62.9%, much higher than the limit of 25%, and a sensitive ECL imaging method was thus proposed for simultaneous high-throughput detection of mucin1-specific sialic acid and fucose on cells by combining a Nt.BbvCI-aided cleavage recycling to obtain the detection samples, and a DNA array to capture the detection samples and then recognize the ECL probes. This method showed good reliability and could be expanded to detect the glycans on different proteins by altering the protein aptamer sequence. This work charts a fresh course for exploiting highly efficient ECL emitters and extends their applications in ECL bioanalysis.

electrochemiluminescence, aggregates, thermally activated delayed fluorescence, biosensors, protein-specific glycoforms, cell surface glycans

Citation: Wang C, Tang Z, Li Y, Li M, Xie H, Ju H. Aggregation of thermally activated delayed fluorescence molecules to boost solid electrochemiluminescence efficiency for biosensing of protein-specific glycoforms. *Sci China Chem*, 2025, 68, https://doi.org/10.1007/s11426-024-2523-2

1 Introduction

Electrochemiluminescence (ECL) is a luminescence phenomenon that occurs when electrochemically generated excited species return to the ground state (S_0) [1–4]. Traditional ECL nanoemitters generally suffer 75% excitation energy loss as they rely solely on the exciton transitions from the lowest excited singlet state (S_1) to S_0 for light emission, while the exciton transitions from the lowest excited triplet state (T_1) to S_0 are non-radiative [5]. Improving the exciton utilization efficiency and fluorescence quantum yield (Φ_{PL}) has become a key to enhancing the ECL efficiency (Φ_{ECL}) of nanoemitters [6]. In order to harvest both singlet and triplet excitons for ECL emission, our previous work reported a dual ECL emissions mechanism of black phosphorus quantum dots from both S_1 and T_1 to S_0 transitions, but both the Φ_{PL} and the Φ_{ECL} were unsatisfied [7]. The reverse intersystem crossing (RISC) of T_1 excitons to S_1 excitons due to the small S_1-T_1 energy gap (ΔE_{ST}) in thermally activated delayed fluorescence (TADF) materials provides a promising

*Corresponding author (email: hxju@nju.edu.cn)

way to boost the exciton utilization efficiency and break through the 25% limit [8–10]. Thus, we synthesized the polymer dots (Pdots) featuring TADF to achieve high exciton utilization efficiency and an Φ_{ECL} of 49.9% *vs.* $[Ru(bpy)_3]^{2+}$ [11]. However, both S_1 and T_1 of TADF Pdots are charge transfer states with low Φ_{PL} [10], and the RISC process was relatively sluggish due to the ΔE_{ST} of 0.0848 eV [12], which might cause triplet-triplet annihilation (TTA) of long-lived triplet excitons (Scheme 1a, left) [13]. Therefore, it is necessary to minimize the S_1-T_1 energy gap for accelerating the RISC and avoiding the TTA of triplet excitons.

When two neighboring phenyl rings get closer to allow their electron communication, the energy gap between the excited states can be decreased, thus the aggregates generally show enhanced Φ_{PL} [14,15]. More interestingly, the highly twisted conformations give rise to extremely small ΔE_{ST} values [16–18]. Inspired by these results, this work used DMAC-TRZ, a previously reported TADF molecule [19] with a twisted conformation and high Φ_{PL}, as a model to design an aggregation strategy for TADF molecules. This strategy could be conveniently performed by increasing the water content in tetrahydrofuran (THF) solution of DMAC-TRZ (Scheme 1b). Compared to traditional TADF materials [5] and TADF Pdots [11], the aggregated DMAC-TRZ possessed much smaller ΔE_{ST} (0.011 eV) and thus rapid RISC process for alleviation of exciton annihilation (Scheme 1a, right), which greatly improved the triplet exciton utilization for reducing excitation energy loss. Owing to the high Φ_{PL} of DMAC-TRZ, the aggregates yielded an Φ_{ECL} of 62.9% relative to 1 mmol L^{-1} $[Ru(bpy)_3]^{2+}$/10 mmol L^{-1} tripropylamine (TPrA) after they were coprecipitated with poly(styrene-*co*-maleic anhydride) (PSMA, a carboxyl-functionalized copolymer) to form DMAC-TRZ/PSMA (DP) NPs,

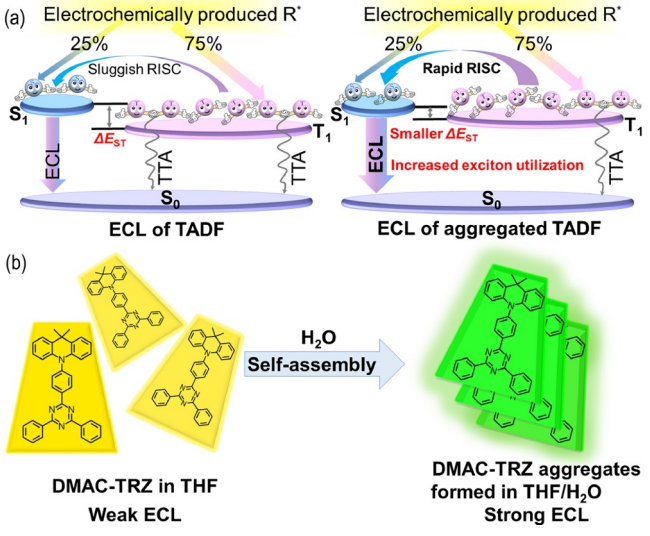

Scheme 1 (Color online) Schematic diagrams of (a) ECL processes of TADF and TADF aggregates, and (b) aggregation of DMAC-TRZ by adding water to THF.

indicating a breakthrough in solid ECL efficiency. Benefitting from the high ECL efficiency of DP NPs, two sensitive ECL probes were thus designed for imaging detection of mucin1 (MUC1)-specific sialic acid (Sia) and fucose (Fuc) on cells.

Cell surface glycoforms play crucial roles in intercellular recognition, adhesion and signaling, and have emerged as potential biomarkers [20,21]. During carcinogenesis, MUC1 is abnormally glycosylated to over-express Sia and Fuc [22,23]. Deciphering MUC1-specific glycans can provide crucial insights for cancer diagnosis. However, the current ECL analysis of glycans cannot detect cell surface protein-specific glycoforms due to inadequate glycoprotein recognition and the lack of efficient ECL emitters [24–27]. By integrating metabolic labeling, nicking endonuclease Nt. BbvCI-aided cleavage recycling to collect the targeted glycans information, this work developed a high-throughput ECL imaging platform for simultaneous detection of protein-specific glycoforms on the cell surface, which achieved ECL visualized analysis of Sia and Fuc on MUC1 from different cell lines, and demonstrated the applications of highly efficient organic ECL emitters in ECL bioanalysis.

2 Experimental

2.1 Materials, reagents and apparatus

The materials, reagents, and apparatus are presented in the Supporting Information online.

2.2 Synthesis of DMAC-TRZ and its aggregates

DMAC-TRZ was prepared according to a previous work [28]. After the mixture of K_2CO_3 (2.0040 g), palladium(II) acetate (0.0530 g), 9,9-dimethyl-9,10-dihydroacridine (1.0046 g), 2-(4-bromophenyl)-4,6-diphenyl-1,3,5-triazine (1.9414 g), and tri-*tert*-butylphosphine (0.4 g) in 50 mL toluene was stirred in a Schlenk tube at 115 °C for 48 h under an argon atmosphere, the formed product was extracted with dichloromethane and purified by silica gel column chromatography with petroleum ether/dichloromethane as eluent to obtain 0.7512 g DMAC-TRZ (yield 86%). Proton nuclear magnetic resonance (^{1}H NMR) (400 MHz, Chloroform-d) δ = 9.04–9.02 (d, J = 8.5 Hz, 2H), 8.83–8.81 (d, J = 6.5 Hz, 4H), 7.62–7.48 (m, 10H), 6.99–6.95 (m, 4H), 6.39–6.37 (d, J = 7.8 Hz, 2H), and 1.73 (s, 6H).

The aggregates of DMAC-TRZ were prepared by adding a THF solution of DMAC-TRZ (0.3 mL, 1 mg mL^{-1}) to THF/H_2O (2.7 mL, with appropriate volume ratios) [29].

2.3 Preparation of DP NPs and ECL probes

DP NPs were prepared through reprecipitation according to

previous work [11]. After 2.5 mL THF solutions of 50 μg mL^{-1} DMAC-TRZ and 10 μg mL^{-1} PSMA were ultrasonically degassed at RT for 20 min, respectively, they were successively added into 10 mL of water with sonication for another 30 s. The presence of PSMA could form carbonxyl groups on the surface of DP NPs for improving the hydrophilicity and biocompatibility and the conjugation of DNA-NH_2 to DP NPs. After the THF was removed via rotary evaporation under vacuum, the resulting solution was filtrated via a 0.22 μmol L^{-1} poly(ether sulfones) syringe filter to obtain carboxyl DP NPs dispersion.

For the preparation of ECL probe 1 or 2, 600 μL dispersion of DP NPs was mixed completely with polyethylene glycol (PEG, 5% w/v, 12 μL) and 4-(2-hydroxyethyl)-1-piperazineethanesulfonic acid (HEPEs, 1 mol L^{-1}, 12 μL), and the pH was adjusted to 7.4 with 0.1 mol L^{-1} NaOH. The presence of PEG could prevent non-specific adsorption of biomolecules. Then Capture DNA1 or Capture DNA2 (100 μmol L^{-1}, 40 μL) and freshly prepared EDC (10 mg mL^{-1}, 24 μL) were injected into the mixture and stirred for 24 h. To remove free Capture DNA, the obtained mixture was separated by ultrafiltration six times, and the product was diluted to an appropriate concentration for subsequent experiments.

2.4 Preparation of ECL imaging array

After a porous sticker was pasted on Au/ITO to form a good array, each well of the array was modified with 3 μL of H_1 or H_2 (2 μmol L^{-1}), which was annealed at 10 μmol L^{-1} and mixed with an equal volume of tris(2-carboxyethyl)phosphine (TCEP) (1 mmol L^{-1}) to reduce disulfide bond for 1 h, to incubate at 37 °C for 2 h. The modified Au/ITO well was washed carefully with phosphate buffer saline (PBS) (pH 7.4), and incubated with 3 μL of 6-hydroxy-1-hexanethiol (MCH, 0.1 mmol L^{-1}) for 1 h to block the unmodified sites. After washing thrice, the DNA array (H/MCH/Au/ITO) was ready for ECL imaging detection.

2.5 Cell culture and treatments

MCF-7 cells were cultured in RPMI-1640 media supplemented with 10% FBS, streptomycin (0.1 mg mL^{-1}) and penicillin (0.1 mg mL^{-1}). HepG2 cells were cultured in DMEM supplemented with 10% FBS, streptomycin (0.1 mg mL^{-1}), and penicillin (0.1 mg mL^{-1}). MDA-MB-231 cells were cultured in Leibovitz's L-15 media supplemented with 10% FBS, streptomycin (0.1 mg mL^{-1}), and penicillin (0.1 mg mL^{-1}). All these cells were grown at 37 °C in a humidified atmosphere containing 5% CO_2 and maintained at densities between 5×10^5 and 2×10^6 cells mL^{-1}.

To verify the specificity of P/B towards MUC1, MCF-7 (MUC1-positive) and HepG2 (MUC1-negative) cells were separately seeded on four-well confocal dishes, treated with 10% goat serum at 37 °C for 30 min, and incubated with FAM-Apt (1.0 μmol L^{-1}), FAM-P/B (1.0 μmol L^{-1}/1.5 μmol L^{-1}), and FAM-Ran (1.0 μmol L^{-1}) at 4 °C for 30 min to collect the confocal laser scanning microscopic (CLSM) signals of FAM on cell surface under 488 nm excitation. siRNA transfection for examining the specificity of the proposed ECL imaging method toward MUC1 was carried out by incubating the cells with culture media containing Ac_4ManNAz (40 μmol L^{-1}, for the metabolic engineering introduction of azide-modified Sia onto cell surface), Ac_4FucNAl (40 μmol L^{-1}, for the metabolic engineering introduction of alkyne-modified Fuc onto cell surface), and 10 μmol L^{-1} siRNA dissolved in transfection complex for 48 h. The BAG (*O*-glycosylation inhibitor) or TM (*N*-glycosylation inhibitor) treatment of cells for verifying the specificity of the proposed method to *O*-glycans was performed by incubating the cells with a mixture of Ac_4ManNAz (40 μmol L^{-1}), Ac_4FucNAl (40 μmol L^{-1}), and BAG (2.5 mmol L^{-1}) or TM (1.0 μmol L^{-1}) in culture medium in a CO_2 incubator at 37 °C for 48 h. The α2-3,6,8,9 neuraminidase A (NEU) or α1-2,4,6 fucosidase (AFU) treatment for verifying the labeling specificity to Sia and fucose Fuc was performed by incubating the cells with a mixture of Ac_4ManNAz (40 μmol L^{-1}) and Ac_4FucNAl (40 μmol L^{-1}) for 48 h, and then treated at 37 °C with NEU (0.2 units mL^{-1}) for 30 min or AFU (0.5 units mL^{-1}) for 60 min.

2.6 Sample collection for imaging cell surface protein-specific glycoforms

After different amounts of cells that were seeded on 96-well plates were incubated with culture medium containing Ac_4ManNAz (40 μmol L^{-1}) and Ac_4FucNAl (40 μmol L^{-1}) in a CO_2 incubator at 37 °C for 48 h to perform the metabolic labeling of Sia and Fuc moieties, they were fixed with cold methanol at 4 °C for 15 min, washed with PBS, blocked with 10% goat serum at 4 °C for 30 min, treated with G_1 (10 μmol L^{-1}) at 4 °C for 30 min, and incubated with 50 mmol L^{-1} TCEP at RT for 10 min to quench the unreacted azide. The G_1 bound cells were then incubated with a mixture of $CuSO_4$ (100 μmol L^{-1}), BTTAA (600 μmol L^{-1}), G_2 (10 μmol L^{-1}) and freshly prepared sodium ascorbate (SA) solution (2.5 mmol L^{-1}) at RT for 5 min to label the Fuc group. After washing and incubating these cells with an MUC1 protein probe (B/P, 1.5 μmol L^{-1}/1.0 μmol L^{-1}) at 4 °C for 30 min and washing with PBS, they were further treated with the mixture of initiate DNA (7.5 μmol L^{-1}) and Nt.BbvCI (600 U mL^{-1} in 1 × Cutsmart buffer) at 37 °C for 90 min to perform the Nt.BbvCI-aided cleavage recycling, which produced a sample solution containing S_1-DNA and S_2-DNA for ECL imaging of MUC1-specific glycoforms.

2.7 ECL imaging detection of MUC1-specific glycoforms

3 μL of the sample solutions containing S_1-DNA and S_2-DNA were dropped in different wells of DNA array (H_1/MCH/Au/ITO or H_2/MCH/Au/ITO) to incubate at 37 °C for 1 h for capturing the corresponding S-DNA. After washing carefully thrice, 3 μL of DP NPs-Capture DNA1 (ECL probe 1) or DP NPs-Capture DNA2 (ECL probe 2) were introduced on the corresponding surface respectively to hybridize with H_1 or H_2 for 1.5 h, followed by washing row-by-row for thrice via gently dropping a washing buffer (10 mmol L^{-1} PBS, pH 7.4) to avoid cross-contamination and then drying at 37 °C for 15 min to carry out the ECL imaging detection. ECL imaging was operated on a self-made ECL imaging system equipped with a focus len (EF 50 mm f/1.2L USM, Canon), an electron multiplying charge-coupled device (EMCCD, iXon Ultra, Andor, UK), and a CHI-660D electrochemical workstation along with an imaging cell including Au/ITO electrode as working, Ag/AgCl wire as a reference and Pt wire as counter electrodes in a dark box. 0.1 mol L^{-1} pH 7.4 PBS containing 25 mmol L^{-1} triethanolamine (TEOA) as a coreactant was employed for ECL imaging. ECL images were recorded at an exposure time of 31 s by cyclic voltammetric scanning between 0–+1.5 V at 0.1 V s^{-1} and then analyzed by ImageJ software.

2.8 CLSM imaging of MUC1-specific Sia and Fuc

After MCF-7 cells were metabolically labelled with F_1-G_1-Q_1 and F_2-G_2-Q_2, they were incubated with B/P (1.5 μmol L^{-1}/1.0 μmol L^{-1}) at 4 °C for 30 min, and treated with initiate DNA (7.5 μmol L^{-1}) and Nt.BbvCI (600 U mL^{-1} in 1 × Cutsmart buffer) at 37 °C for 90 min to perform CLSM imaging under 488 and 649 nm excitation, respectively.

3 Results and discussion

3.1 Photophysical property of DMAC-TRZ

DMAC-TRZ was synthesized via Buchwald-Hartwig amination [28] (Figure 1a) and verified by ^{1}H NMR spectroscopy (Figure S1, Supporting Information online). The DMAC moiety as electron donor and the TRZ moiety as electron acceptor gave rise to a twisted arrangement with a dihedral angle of 87° (Figure 1b), indicating a twisted conformation, which enhanced the separation of frontier orbitals and suppressed aggregation-caused quenching. The UV-vis absorption spectra of DMAC-TRZ in different solvents showed absorption at 380 nm, while the fluorescence (FL) emission displayed a solvent polarity-driven bathochromic shift (Figure 1c, d), suggesting its charge transfer property [30]. The transient FL spectra of DMAC-TRZ (Figure 1e) exhibited a dual-component decay with a temperature-dependent delayed component, proving its TADF property [30]. From the onsets of FL and phosphorescence (PL) spectra of DMAC-TRZ (Figure 1f), the ΔE_{ST} was measured to be 0.030 eV, which was lower than the limit of ca. 0.1 eV [18] and that of TADF Pdots [11]. To get deep insights into the TADF mechanism, the lowest ten singlet and triplet ex-

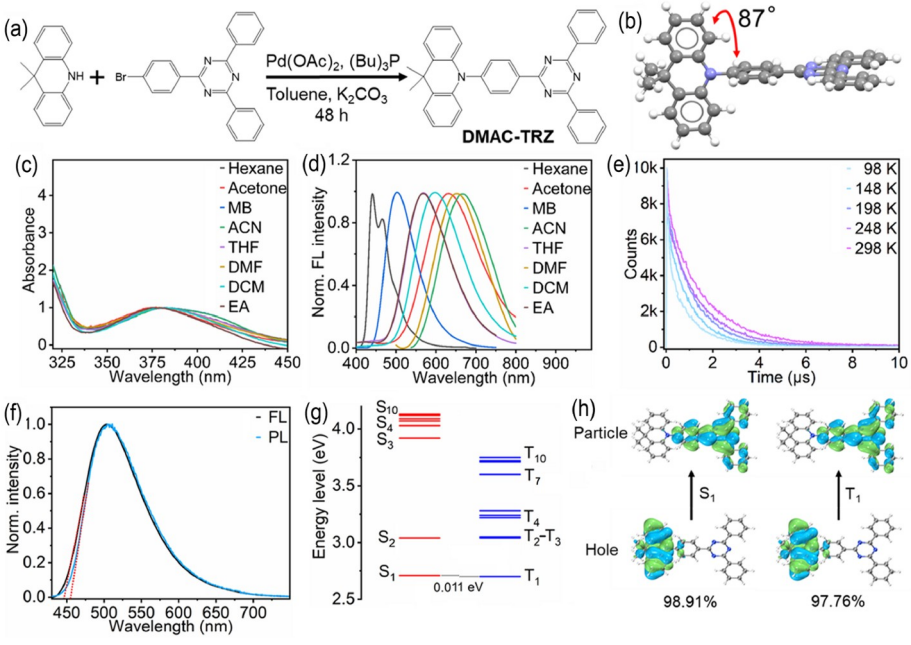

Figure 1 (Color online) (a) Synthesis route and (b) geometric conformation of DMAC-TRZ. (c) UV-vis absorption and (d) FL spectra of DMAC-TRZ in different solvents. (e) FL decay, and (f) FL, phosphorescence (77 K) spectra of DMAC-TRZ in toluene. (g) Energy diagram of excited states of DMAC-TRZ, including the lowest ten singlet and triplet excited states at M06-2x(D3)/def2-TZVP level. (h) Natural transition orbitals of DMAC-TRZ in S_1 and T_1 states (the percentage represents transition possibility).

cited states of DMAC-TRZ were calculated (Figure 1g, Table S1, Supporting Information online). The narrow theoretical ΔE_{ST} of 0.011 eV made the RISC more rapid, leading to sufficient utilization of triplet excitons via the rapid RISC process. Additionally, the well-separated holes and particle distributions in both S_1 and T_1 of DMAC-TRZ (Figure 1h) affirmed their charge transfer characteristics.

The photophysical property of DMAC-TRZ was further studied by recording its FL spectra in a THF/water mixture with varying water fractions (f_w) (Figure S2a). With the increasing f_w, the FL intensity of DMAC-TRZ declined and then drastically increased when $f_w \geqslant 50\%$ (Figure S2b), while the FL emission showed a red-shift up to 624 nm at $f_w = 50\%$ and then blue-shifted to 518 nm at $f_w = 90\%$ (Figure S2b), indicating the formation of aggregates in the THF/water mixture when $f_w > 50\%$ [31]. When f_w increased from 70% to 90%, the delayed FL lifetime was also elongated (Figure S2d), indicating that the aggregation was beneficial for prolonging the FL lifetime [32]. Moreover, the ECL intensity of DMAC-TRZ in the presence of TEOA as coreactant increased upon its aggregation and then coating the aggregates on a glassy carbon electrode (GCE) (Figure S2e, f), revealing that the aggregation of DMAC-TRZ could enhance its ECL emission.

3.2 Characterization of DP NPs

To investigate the ECL behavior of DMAC-TRZ aggregates, DP NPs were prepared by using PSMA as a copolymer (Figure 2a), which exhibited a spherical morphology with an average diameter of 25 nm (Figure 2b–d). The DP NPs showed bright green emission under 365 nm irradiation (Figure 2e), and the Φ_{PL} was measured to be 87.5%, surpassing those of 26.2% and 73.7% for DMAC-TRZ in THF and TADF Pdots in water [11], respectively. Although the FL emission peak of DP NPs was blue-shifted to 507 nm compared to 574 nm of DMAC-TRZ in THF due to the aggregation of DMAC-TRZ in the presence of H_2O (Figure 2f), the UV-vis absorption spectrum was similar to that of DMAC-TRZ in THF, and the FL emission was also close to that of DMAC-TRZ aggregates in THF/water mixture at $f_w = 90\%$, indicating that the influence of reprecipitation on the absorption and emission of DMAC-TRZ aggregates was negligible.

3.3 ECL property of DP NPs

The CV curves of DP NPs/GCE showed an irreversible oxidation peak at ca. +1.26 V and a reduction wave at potentials more negative than −1.28 V, which gave rise to an intensive ECL emission at about +0.8 V (Figure S3a, b), indicating that electrochemically generated DP NPs$^{\cdot-}$ were stable enough to react with the following generated DP NPs$^{\cdot+}$ for producing annihilation ECL [7], which also led to a stronger ECL emission for initial cathodic scanning (Figure S3b). This conclusion could also be demonstrated by the

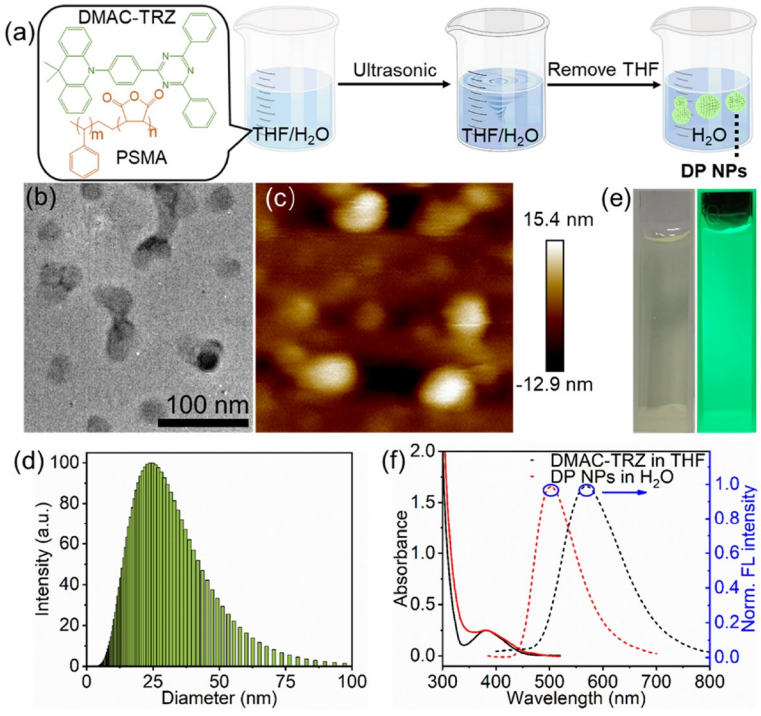

Figure 2 (Color online) (a) Schematic diagram of the preparation of DP NPs. (b) Transmission electron microscope (TEM), (c) atomic force microscope (AFM), and (d) dynamic light scattering (DLS) characterization of DP NPs. (e) Photographs of DP NPs dispersion under daylight (left) and 365 nm irradiation (right). (f) UV-vis absorption and FL spectra of DP NPs in water and DMAC-TRZ in THF.

ECL transients of DP NPs. When the pulse potential was switched from −2.0 to +1.5 V, the transient ECL intensity was greater than that of from +1.5 to −2.0 V (Figure S3c, d).

To elucidate the ECL efficiency of DP NPs, the ECL behavior of coreactant was further studied. TEOA was chosen as the optimal coreactant (Figure 3a) because the hydroxyethyl groups in TEOA could catalyze the oxidation of amines [33]. The ECL intensity of DP NPs increased with the increasing concentration of TEOA from 10 to 25 mmol L^{-1}, and then reached a plateau value at 25 mmol L^{-1}, which was selected as the optimal concentration (Figure 3b). At bare GCE, TEOA showed an oxidation peak at around +1.20 V, which was also observed at DP NPs/GCE (Figure 3c). Meanwhile, the DP NPs/GCE showed an oxidation peak of DP NPs at +1.25 V, which resulted in an intensive ECL emission at +1.25 V (Figure 3d). Therefore, the anodic ECL of DP NPs followed an "oxidative-reduction" pathway (Figure 3e), in which TEOA and DP NPs were oxidized successively to produce $TEOA^{\cdot+}$ and $DP\ NPs^{\cdot+}$, then the charge transfer between $TEOA^{\cdot}$ and $DP\ NPs^{\cdot+}$ produced the excited singlet and triplet states of DP NPs (^{1}DP NPs* and ^{3}DP NPs*), followed by rapid transfer of triplet excitons to singlet state via RISC to produce ECL emission upon the radiative relaxation of ^{1}DP NPs*. The ECL emission wavelength of DP NPs was close to its FL emission wavelength (Figure S4a), indicating the same excited states in ECL and FL processes. With 10 mmol L^{-1} TPrA as coreatant, the Φ_{ECL} of DP NPs was calculated to be 62.9% *vs.* 1 mmol L^{-1} $[Ru(bpy)_3]^{2+}$ (Figure S4b, c, Table S2), much higher than those of fluorescent Pdots [34–37], and also higher than those of TADF Pdots [11] and hot exciton nanomaterial [38] (Table S3), suggesting a breakthrough in solid Φ_{ECL} and the huge potential of DP NPs in ECL imaging analysis.

3.4 Feasibility of ECL detection of MUC1-specific Sia and Fuc

To verify the ECL imaging application, DNA-functionalized DP NPs were prepared as ECL probes **1** or **2** by covalently conjugating DP NPs with Capture DNA **1** or **2**, respectively. Upon the conjugation of DP NPs with DNA, the absorption peak of DP NPs-DNA blue-shifted slightly due to the partial overlap between the absorption peaks of DNA and DP NPs, and the Zeta potential experienced a noticeable decline

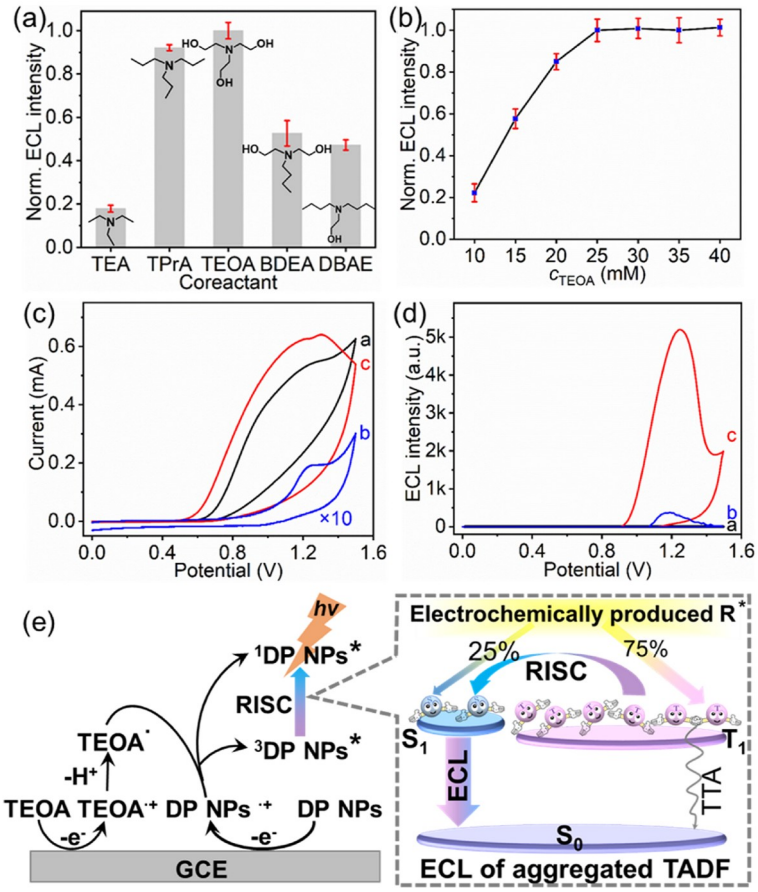

Figure 3 (Color online) (a) Normalized ECL intensity of DP NPs/GCE in 0.1 mol L^{-1} PBS containing 25 mmol L^{-1} TEA, TPrA, TEOA, BDEA, or DBAE (n = 3). (b) Effect of TEOA concentration on ECL intensity of DP NPs/GCE (n = 3). (c) CV and (d) ECL curves of GCE and DP NPs/GCE in 0.1 mol L^{-1} PBS (pH 7.4) in the absence or presence of 25 mmol L^{-1} TEOA. (e) ECL mechanism of DP NPs.

(Figure S5), demonstrating the successful preparation of ECL probes.

To realize the simultaneous detection of MUC1-specific Sia and Fuc, two glycan probes (G_1 and G_2) and a protein probe for MUC1 (B/P) were designed (Table S4), in which G_1 and G_2 contained Nt.BbvCI recognition sites [39], and P contained MUC1-binding aptamer S2.2 [40] and was pre-blocked by blocker DNA (B) to hybridize with G till it was released by a strand replacement reaction of initiate DNA with B/P (Scheme 2a). After G_1 and G_2 were metabolically labeled to Sia and Fuc, respectively, and B/P was bound to MUC1 on the cell surface, the addition of Nt.BbvCI and initiate DNA could release P to trigger Nt.BbvCI-aided cleavage recycling, which obtained the detection samples containing S_1-DNA and S_2-DNA that represent the amounts of Sia and Fuc on MUC1, respectively. On H_1 or H_2 modified Au/ITO, S_1-DNA and S_2-DNA could be captured to open H_1 or H_2 for binding Capture DNA1 or DNA2 functionalized DP NPs, respectively, which led to sensitive ECL signals for analysis of protein-specific glycans (Scheme 2b).

Polyacrylamide gel electrophoresis (PAGE) was first employed to explore the feasibility of simultaneous detection of MUC1-specific Sia and Fuc. Upon the addition of initiate DNA into P/B, P was successfully released from P/B (Figure S6, lanes 5 and 6), suggesting the feasibility of a toehold-mediated strand displacement reaction. The incubation of Nt.BbvCI with P/G_1 produced cleaved G_1, and this phenomenon became more obvious when the concentration of G_1 was doubled (Figure S6, lanes 8 and 9), demonstrating the feasibility of Nt.BbvCI-aided cleavage recycling. Moreover, in the absence of initiate DNA and Nt.BbvCI, B/P failed to react with G_1, whereas the addition of initiate DNA caused the liberation of P from B/P to open G_1 (Figure S7a, lanes 1 and 2), and the coaddition of initiate DNA and Nt.BbvCI led to the cleavage of G_1 even when the concentrations of B/P and initiate DNA were lowered to 10% (Figure S7a, lanes 3 and 4). This was also proved by FL measurements on a system containing F-G-Q, B/P, initiate DNA and Nt.BbvCI (Figure S7b). To achieve the simultaneous detection of two protein-specific glycans, it was essential to ensure the absence of cross-talk between the two glycan probes as well as the two detection systems. PAGE analysis (Figure S8) revealed that G_1' or the opened G_1' could not hybridize with G_2', and S_1 failed to open H_2, thereby enabling the simultaneous detection of MUC1-bound terminal Sia and Fuc.

The specificity of P/B to MUC1 was verified by CLSM imaging of MUC1-positive MCF-7 and MUC1-negative HepG2 cells using fluorescein (FAM) labeled MUC1 aptamer (FAM-Apt), protein probe (FAM-P/B) and random-sequenced DNA (FAM-Ran). Compared to the incubation of MCF-7 cells with FAM-Ran, bright fluorescence was observed upon incubation with either FAM-Apt or FAM-P/B (Figure S9, left), indicating the high specificity of P/B towards MUC1. This was also supported by the lack of

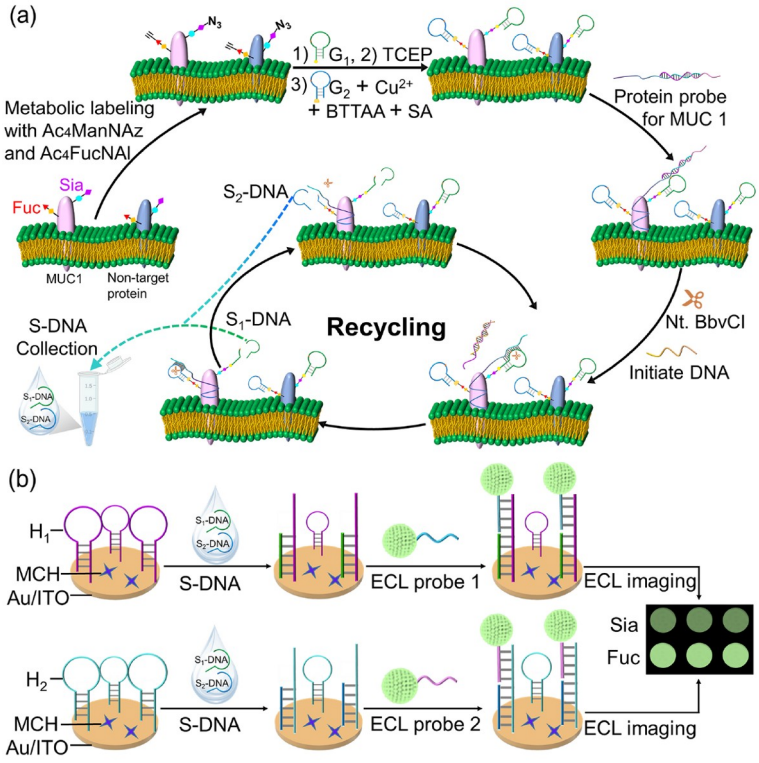

Scheme 2 (Color online) Schematic diagrams of (a) sample collection of cell surface protein-specific glycoforms by metabolic labeling and Nt.BbvCI-aided cleavage recycling, (b) ECL imaging array for detection of MUC1-specific Sia and Fuc.

fluorescence on MUC1-negative HepG2 cells under the same treatment (Figure S9, right). The toehold-mediated strand displacement and Nt.BbvCI-aided cleavage recycling on live cells was further verified by dual-color CLSM imaging using F_1-G_1-Q_1 and F_2-G_2-Q_2 as the glycan probes. After the glycan probes were specifically assembled on cells, the addition of B/P and initiate DNA led to a weak FL due to the partial unfolding of G by P, while the further addition of Nt.BbvCI drove the Nt.BbvCI-aided cleavage recycling and thus produced a bright FL (Figure S10), revealing the feasibility of collecting S_1-DNA and S_2-DNA. The electrochemical impedance spectra confirmed the hairpin modification of Au/ITO, and the capture of S_1-DNA or S_2-DNA and the binding of ECL probes on the modified Au/ITO (Figure S11).

3.5 ECL imaging detection of MUC1-specific Sia and Fuc

Before the detection of MUC-specific Sia and Fuc, the hairpin concentration and the incubation time of ECL probes were optimized to be 2.0 μmol L^{-1} and 90 min, respectively (Figure S12). After S-DNA and then ECL probe were assembled on H_1/MCH/Au/ITO or H_2/MCH/Au/ITO, the plot of ECL intensity (*I*) *vs.* S-DNA concentration showed a proportional relationship: $I = k_1 c_{DNA} + b_1$. As a different concentrations of cells could release different amounts of S-DNA after Nt.BbvCI-aided cleavage recycling, the *I* value was also proportional to the concentration of analyzed cells: $I = k_2 c_{cell} + b_2$. From these equations, the average amount of released protein-specific S-DNA per cell (a_{DNA}) could be calculated with $a_{DNA} = k_2/k_1$. Under optimal conditions, MUC1-specific Sia on each MCF-7 or MDA-MB-231 cell was detected to be 5.0×10^6 or 3.8×10^6, respectively (Figure 4a–c). Given that each MCF-7 and MDA-MB-231 cell expressed 1.3×10^5 and 7.2×10^4 MUC1 [41], one MUC1 on MCF-7 or MDA-MB-231 cells was modified by approximately 38 and 53 Sia, respectively. Similarly, one MUC1 on MCF-7 or MDA-MB-231 cells bound 69 and 101 Fuc, respectively (Figure 4d–f, Table S5).

After siRNA-induced downregulation of MUC1 expression, the ECL signals responsive to cell surface MUC1-specific Sia and Fuc obviously attenuated (Figure 4g), verifying the specificity of the proposed ECL imaging method. Since MUC1 is a highly *O*-glycosylated protein [22], the ECL signals responsive to cell surface MUC1-specific Sia and Fuc exhibited a significant decrease after treating the cells with *O*-glycosylation inhibitor BAG and then collecting the S-DNA sample (Figure 4h), while *N*-glycosylation inhibitor TM treatment did not obviously change the ECL

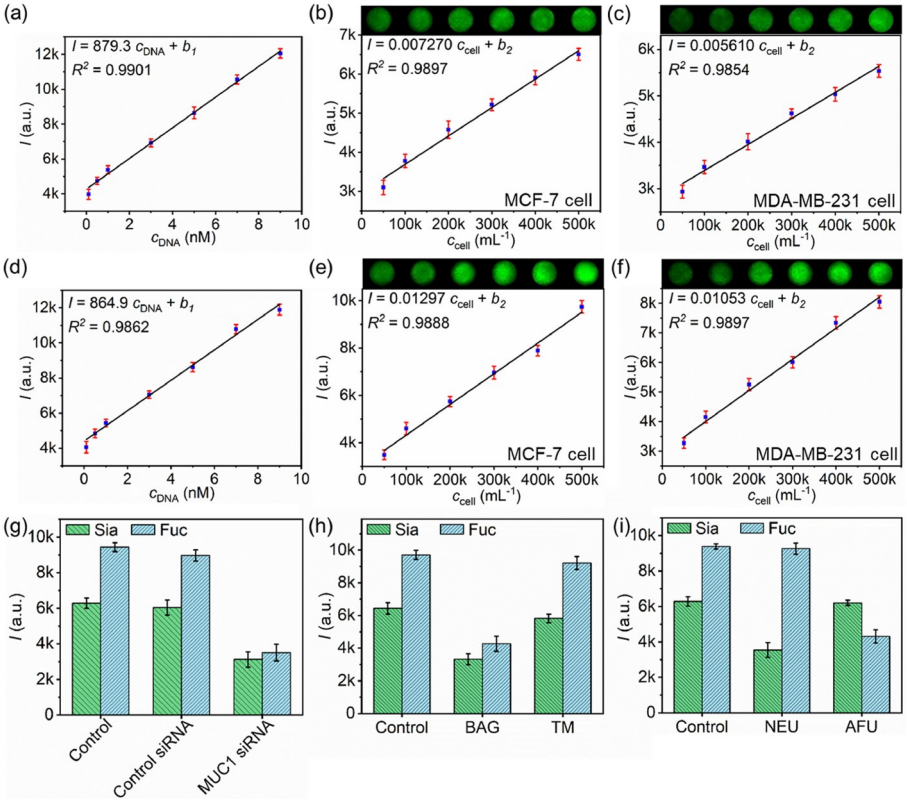

Figure 4 (Color online) Calibration curves for S_1-DNA (a) and S_2-DNA (d) detection with ECL imaging array. ECL images and plots of ECL intensity *vs.* MCF-7 (b, e) and MDA-MB-231 (c, f) cells concentration for MUC1-specific Sia (b, c) and Fuc (e, f) detection. Specificity of the proposed ECL imaging method for cell surface MUC1-specific glycans upon siRNA-induced MUC1 downregulation (g), BAG and TM (h), and NEU and AFU (i) treatments. Control indicates no treatment ($n = 5$).

signals, inferring the good specificity of the proposed method to *O*-glycans Sia and Fuc. The labeling specificity to Sia and Fuc was further demonstrated by treating the cells with neuraminidase (NEU) or α-L-fucosidase (AFU) to cleave Sia or Fuc respectively, which led to a significant decrease of ECL signals (Figure 4i).

4 Conclusions

This work developed an aggregation strategy of TADF molecules to minimize the S_1-T_1 energy gap ΔE_{ST} of the ECL process for accelerating the reverse intersystem crossing of triplet excitons to the excited singlet state. This strategy greatly increased the exciton utilization and the quantum yield of TADF molecules, and thus produced highly efficient ECL nanoemitters, which showed a ground-breaking solid Φ_{ECL} of 62.9%. Based on the strong ECL emission of the obtained nanoemitters, a high-throughput ECL imaging method was developed for the simultaneous analysis of two MUC1-specific glycans on cells by integrating metabolic labeling and Nt.BbvCI-aided cleavage recycling to collect the targeted glycans information. The reliability of the proposed detection method was demonstrated through different cell treatments. By altering the protein aptamer sequence, this method could be expanded to detect the glycans on different proteins. This work provides a new path to exploit highly efficient ECL nanoemitters for achieving their practical applications.

Acknowledgements This work was supported by the National Natural Science Foundation of China (21827812, 21890741).

Conflict of interest The authors declare no conflict of interest.

Supporting information The supporting information is available online at http://chem.scichina.com and http://link.springer.com/journal/11426. The supporting materials are published as submitted, without typesetting or editing. The responsibility for scientific accuracy and content remains entirely with the authors.

1 Cao Z, Li C, Shu Y, Zhu M, Su B, Qin H, Peng X. *J Am Chem Soc*, 2023, 145: 26425–26434
2 Feng Y, Wang N, Ju H. *Sci China Chem*, 2022, 65: 2417–2436
3 Liu Z, Qi W, Xu G. *Chem Soc Rev*, 2015, 44: 3117–3142
4 Zhang Y, Xu Y, Li J, Chen R, Chen W, Peng H. *TrAC Trends Anal Chem*, 2024, 178: 117812
5 Ishimatsu R, Matsunami S, Kasahara T, Mizuno J, Edura T, Adachi C, Nakano K, Imato T. *Angew Chem Int Ed*, 2014, 53: 6993–6996
6 Zhang B, Kong Y, Liu H, Chen B, Zhao B, Luo Y, Chen L, Zhang Y, Han D, Zhao Z, Tang BZ, Niu L. *Chem Sci*, 2021, 12: 13283–13291
7 Yu S, Du Y, Niu X, Li G, Zhu D, Yu Q, Zou G, Ju H. *Nat Commun*, 2022, 13: 7302
8 Xie Y, Hua L, Wang Z, Liu Y, Ying S, Liu Y, Ren Z, Yan S. *Sci China Chem*, 2023, 66: 826–836
9 Liu Y, Li C, Ren Z, Yan S, Bryce MR. *Nat Rev Mater*, 2018, 3: 18020
10 Li W, Pan Y, Xiao R, Peng Q, Zhang S, Ma D, Li F, Shen F, Wang Y, Yang B, Ma Y. *Adv Funct Mater*, 2014, 24: 1609–1614
11 Wang C, Wu J, Huang H, Xu Q, Ju H. *Anal Chem*, 2022, 94: 15695–15702
12 Rao J, Yang L, Li X, Zhao L, Wang S, Tian H, Ding J, Wang L. *Angew Chem Int Ed*, 2021, 60: 9635–9641
13 Zhang H, Zhang B, Zhang Y, Xu Z, Wu H, Yin P, Wang Z, Zhao Z, Ma D, Tang BZ. *Adv Funct Mater*, 2020, 30: 2002323
14 Zhao Z, Zhang H, Lam JWY, Tang BZ. *Angew Chem Int Ed*, 2020, 59: 9888–9907
15 Zhang JQ, Xu XY, Liu FS, Cao SQ, Gui YX, Su YW, He XY, Liang JY, Zou YQ. *Sci China Chem*, 2024, 67: 2614–2628
16 Zheng K, Ni F, Chen Z, Zhong C, Yang C. *Angew Chem Int Ed*, 2020, 59: 9972–9976
17 Huang J, Nie H, Zeng J, Zhuang Z, Gan S, Cai Y, Guo J, Su S-, Zhao Z, Tang BZ. *Angew Chem Int Ed*, 2017, 56: 12971–12976
18 Lee SY, Yasuda T, Nomura H, Adachi C. *Appl Phys Lett*, 2012, 101: 093306
19 Tsai WL, Huang MH, Lee WK, Hsu YJ, Pan KC, Huang YH, Ting HC, Sarma M, Ho YY, Hu HC, Chen CC, Lee MT, Wong KT, Wu CC. *Chem Commun*, 2015, 51: 13662–13665
20 Chen Y, Ding L, Ju H. *Acc Chem Res*, 2018, 51: 890–899
21 Chen HY. *Sci China Chem*, 2020, 63: 564–588
22 Hollingsworth MA, Swanson BJ. *Nat Rev Cancer*, 2004, 4: 45–60
23 Pearce OMT, Läubli H. *Glycobiology*, 2016, 26: 111–128
24 He Y, Li J, Liu Y. *Anal Chem*, 2015, 87: 9777–9785
25 Wu Y, Gu Q, Wang Z, Tian Z, Wang Z, Liu W, Han J, Liu S. *Anal Chem*, 2024, 96: 2165–2172
26 Zhang L, Wang Y, Tian Q, Liu Y, Li J. *Biosens Bioelectron*, 2017, 89: 1013–1019
27 Zhou B, Qiu Y, Wen Q, Zhu M, Yang P. *ACS Appl Mater Interfaces*, 2017, 9: 2074–2082
28 Lin TA, Chatterjee T, Tsai WL, Lee WK, Wu MJ, Jiao M, Pan KC, Yi CL, Chung CL, Wong KT, Wu CC. *Adv Mater*, 2016, 28: 6976–6983
29 Zhang X, Liu H, Zhuang G, Yang S, Du P. *Nat Commun*, 2022, 13: 3543
30 Naveen KR, Oh JH, Lee HS, Kwon JH. *Angew Chem Int Ed*, 2023, 62: e202306768
31 Gao H, Shi S, Wang S, Tao Q, Ma H, Hu J, Chen H, Xu J. *Aggregate*, 2024, 5: e394
32 Song F, Ou X, Chou TY, Liu J, Gao H, Zhang R, Huang X, Zhao Z, Sun J, Chen S, Lam JWY, Tang BZ. *ACS Nano*, 2022, 16: 6176–6184
33 Liu X, Shi L, Niu W, Li H, Xu G. *Angew Chem Int Ed*, 2007, 46: 421–424
34 Wang Z, Feng Y, Wang N, Cheng Y, Quan Y, Ju H. *J Phys Chem Lett*, 2018, 9: 5296–5302
35 Feng Y, Wang N, Ju H. *Anal Chem*, 2018, 90: 1202–1208
36 Zhang N, Gao H, Jia YL, Pan JB, Luo XL, Chen HY, Xu JJ. *Anal Chem*, 2021, 93: 6857–6864
37 Sun F, Wang Z, Feng Y, Cheng Y, Ju H, Quan Y. *Biosens Bioelectron*, 2018, 100: 28–34
38 Wang C, Cui LJ, Wu J, Hu XF, Wu XT, Cui ZH, Ju HX. *Nano Today*, 2024, 54: 1021
39 Kong RM, Zhang XB, Zhang LL, Huang Y, Lu DQ, Tan W, Shen GL, Yu RQ. *Anal Chem*, 2011, 83: 14–17
40 Ferreira CSM, Matthews CS, Missailidis S. *Tumor Biol*, 2006, 27: 289–301
41 Gao T, Wang B, Shi L, Zhu X, Xiang Y, Anzai J, Li G. *Anal Chem*, 2017, 89: 10776–10782